Science Bulletin 64 (2019) 270–280

Contents lists available at ScienceDirect

Science Bulletin

journal homepage: www.elsevier.com/locate/scib

Article

A novel energy storage system incorporating electrically rechargeable liquid fuels as the storage medium

Haoran Jiang, Lei Wei, Xinzhuang Fan, Jianbo Xu, Wei Shyy, Tianshou Zhao *

Department of Mechanical and Aerospace Engineering, The Hong Kong University of Science and Technology, Clear Water Bay, Kowloon, Hong Kong, China

ARTICLE INFO

Article history:
Received 12 January 2019
Received in revised form 16 January 2019
Accepted 22 January 2019
Available online 25 January 2019

Keywords:
Renewable energy
Energy storage
Batteries
E-fuel energy storage system

ABSTRACT

We propose a novel concept of energy storage that incorporates electrically rechargeable liquid fuels made of electroactive species, known as e-fuels, as the storage medium. This e-fuel energy storage system comprises an e-fuel charger and an e-fuel cell. The e-fuel charger electrically charges e-fuels, while the e-fuel cell subsequently generates electricity using charged e-fuels whenever and wherever on demand. The e-fuel energy storage system possesses all the advantages of conventional hydrogen storage systems, but unlike hydrogen, liquid e-fuels are as easy and safe to store and transport as gasoline. The potential e-fuel candidates have been identified to include inorganic electroactive materials, organic electroactive materials, and suspension of solid electroactive materials. In this work, we demonstrate an example e-fuel energy storage system for large-scale energy storage using inorganic e-fuels composed of V^{2+}/V^{3+} and VO^{2+}/VO_2^+ redox couples, and compare the performance of the e-fuel energy storage system with that of existing technologies. Results show that our e-fuel charger achieves a charge efficiency of as high as ~94%, while the e-fuel cell is capable of delivering a peak power density of 3.4 W cm^{-2}, which is 1.7 times higher than that of hydrogen fuel cells. More excitingly, the e-fuel energy storage system exhibits a round-trip efficiency of 80.0% and an electrolyte utilization of 83.0% at an ultra-high discharge current density of 1,000 mA cm^{-2}, which are 19.9% and 67.3% higher than those of conventional vanadium redox flow batteries. This unprecedented performance allows a 27.0% reduction in the capital cost of the e-fuel energy storage system compared with that of vanadium redox flow batteries.

1. Introduction

The newly approved landmark Paris climate agreement aims to prevent global temperatures from rising another degree Celsius between now and 2100 [1]. Accomplishing this goal will be a herculean task, as it means coming up with a continuous flow of carbon-free power two to three times greater than today's total energy supply to sustain the economic development for a global population approaching 11 billion by the end of the century. Solar and wind energies are two of the largest sustainable sources of carbon-free power, and the past decade has seen remarkable progress in both solar photovoltaics and wind turbines [2]. However, the widespread use of renewables is hindered because the electricity directly obtained from photovoltaics and wind turbines is intermittent and, thus, unreliable. An ultimate solution to solve this issue is to develop off- and micro-grid systems that can store energy to secure an efficient and stable supply of electricity. In addition to the usual requirements of efficiency, scalability, durability, and economy, these energy storage systems should be independent of site, able to operate continuously, and capable of storing energy safely for prolonged periods.

Current and emerging energy storage technologies that might be suited to off- and micro-grid systems include pumped hydro, compressed air, supercapacitors, solid-state batteries, flow batteries, and hydrogen storage, among others. Pumped hydro and compressed air, which employ water or ambient air as the energy-bearing materials, have significant advantages in terms of cost and lifetime. However, these technologies are highly site-dependent and limited by local geography or geology, so they are not easily deployable [3,4]. Supercapacitors have split-second response time, are capable of deep discharge, and can deliver high power, but only for short durations, so they are more suitable for managing power quality than for storing renewables [5]. Solid-state batteries can be used independent of site and are highly energy efficient. They have gained popularity in applications ranging from portable electronic devices to electrical vehicles, but not so in medium- to large-scale applications because of their poor scalability, high cost, short lifetime, and safety concerns [6]. An emerging alternative to solid-state batteries in large-scale

* Corresponding author.
E-mail address: metzhao@ust.hk (T. Zhao).

https://doi.org/10.1016/j.scib.2019.01.014
2095-9273/

application is flow batteries, which represent a promising energy storage technology as they offer excellent scalability, high energy efficiency, and long lifetime. However, current flow batteries have yet to penetrate the market, mainly because of their poor performance, low energy density, and high capital cost [7,8].

For future off- and micro-grid energy storage systems, solar or wind power systems should be able to store energy for days to approximately a week, with or without connections to the electric grid [9]. In this regard, it would be more attractive to convert electricity to fuels to store electricity, since fuels, such as gasoline, are inexpensive to store for periods of a week or more, and are easy to transport. The most developed system based on this concept is the hydrogen storage system, in which hydrogen is employed as the fuel [10]. Hydrogen can be generated locally by electrolysis of water using intermittent solar or wind power. Later, when combined with air in engines or fuel cells, hydrogen can regenerate electricity on demand. However, the low energy efficiency, and the short lifetime of electrolyzers and fuel cells combine to reduce the attractiveness of this technology [11–13]. More fatally, hydrogen is in a gaseous state and is hard to store and transport, which greatly increase the capital cost and lead to severe safety concerns.

To enable the widespread deployment of intermittent and scattered renewables, we propose a novel concept of energy storage that incorporates electrically rechargeable liquid fuels made of electroactive species, known as e-fuels, as the storage medium. This e-fuel energy storage system possesses all the advantages of conventional hydrogen storage systems, but unlike hydrogen, liquid e-fuels are as easy and safe to store and transport as gasoline. The e-fuel energy storage system (e-fuel system), as illustrated in Fig. 1, consists of an e-fuel charger and an e-fuel cell. The e-fuel charger electrically charges e-fuels to store the intermittent electricity harvested with wind turbines and solar photovoltaics in liquid fuels, while the e-fuel cell can generate electricity using charged e-fuels wherever and whenever on demand. The charged and discharged e-fuels are stored in external reservoirs and can be easily transported by pipelines, trucks, or ships. The ease of storing and transporting e-fuel makes the e-fuel system an excellent choice not only for grid-scale energy storage, but also for off-grid power supplies to power sites not on the grid. Unlike all existing rechargeable electrical energy storage systems, which operate in either the charge or discharge mode, the proposed e-fuel system allows simultaneous storage and utilization of energy, as the e-fuel charger and e-fuel cell are operated independently. In addition, the stand-alone power pack even holds the potential to propel next-generation vehicles with not only a safer driving experience, but also a refueling time akin to that of gasoline, at a fraction of the cost of today's lithium-ion batteries.

The potential e-fuels can be made of three categories of electroactive materials, including inorganic materials (*e.g.*, metal ions, halide ions, and metal ionic compounds), organic materials (*e.g.*, quinones, alloxazines, and nitroxyl radicals), and suspensions of particles (named as nanofluid e-fuels, *e.g.*, polysulphide-based nanofluid and metal-ion intercalated nanofluid). In this work, we demonstrate an example e-fuel system for large-scale energy storage with the e-fuels composed of V^{2+}/V^{3+} and VO^{2+}/VO_2^+ redox couples, which are also the electroactive species of conventional vanadium redox flow batteries (VRFBs). In the past decades, the commercialization of VRFBs has been hindered by the low power density, low electrolyte utilization, fast capacity decay, and high capital cost [14–16], due largely to the contradiction of requirements between charge and discharge processes. The e-fuel system overcomes these impediments. Unlike in conventional flow batteries that constrain the charge and discharge processes to one stack, the e-fuel system separates the charge and discharge processes to the e-fuel charger and e-fuel cell, which can be designed, optimized, and operated independently to suppress side reactions, maximize the power density, and increase the electrolyte utilization.

2. Methods

2.1. Electrode fabrication and characterization

Commercially available graphite felts (SGL Group, GFA6 EA) were separated along the cross section, washed with ethanol, and dried in a vacuum oven to act as the starting materials. Highly active graphite felts (HAGF) were prepared by annealing the starting graphite felts in a muffle furnace at 500 °C for 8 h with a heating rate of 5 °C min^{-1} in the ambient air. Traditional VRFB electrodes were prepared by annealing the starting graphite felts in a muffle furnace at 400 °C for 4 h with a heating rate of 5 °C min^{-1} in ambient air. 0.1 mmol Pb was electrodeposited onto the negative electrode of the e-fuel charger by charging it with a 20 mL solution containing 0.3 mol L^{-1} $Fe(SO_3CH_3)_2$ + 0.15 mol L^{-1} $Pb(SO_3CH_3)_2$ + 2.0 mol L^{-1} HSO_3CH_3 as both negative and positive electrolytes. In addition, 0.1 mmol Bi was electrodeposited on the negative electrode of the e-fuel cell by charging it with a 20 mL solution containing 0.1 mol L^{-1} $BiCl_3$ + 3.0 mol L^{-1} HCl and 0.1 mol L^{-1} $VOSO_4$ + 3.0 mol L^{-1} HCl as negative and positive electrolytes, respectively. The surface morphologies of the electrodes were observed by a scanning electron microscope (JEOL-6700 SEM) at an acceleration voltage of 10.0 kV. X-ray photoelectron spectroscopy (XPS) characterization was conducted using Al

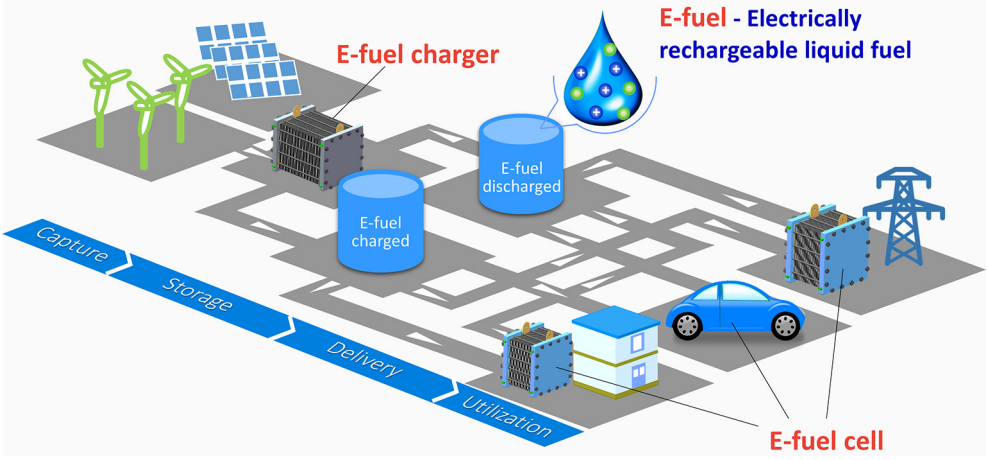

Fig. 1. Schematic of the e-fuel energy storage system.

monochromatic X-rays at a power of 350 W by a Physical Electronics PHI 5600 multi-technique system.

2.2. Assembly of the e-fuel system

The e-fuel system was constructed by connecting an e-fuel charger and an e-fuel cell with two e-fuel tanks. Both the e-fuel charger and the e-fuel cell were assembled by bolting together the following components in the following order: a bakelite plate, an aluminum plate, a gold-coated copper plate, a graphite plate, a negative electrode, a membrane, a positive electrode, a graphite plate, a gold-coated copper plate, an aluminum plate, and a bakelite plate. For the e-fuel charger, one piece of the Pb-modified HAGF was used as the negative electrode, Nafion 212 (50 μm, Dupont, USA) was used as the membrane, and one piece of the HAGF was used as the positive electrode. For the e-fuel cell, one piece of the Bi-modified HAGF was used as the negative electrode, Nafion 211 (25 μm, Dupont, USA) was used as the membrane, and one piece of the HAGF was used as the positive electrode. The active areas of all electrodes were 2.0 cm × 2.0 cm. During the experiments, the e-fuel was charged in the e-fuel charger, totally transferred to the tanks, discharged in the e-fuel cell, and finally totally transferred back to the tanks to finish a cycle. Here, V^{2+}/V^{3+} and VO^{2+}/VO_2^+ redox couples were adopted as an example of e-fuels, and 40 mL solutions containing 1.07 mol L^{-1} V^{3+} + 3.0 mol L^{-1} H_2SO_4 and 1.07 mol L^{-1} VO^{2+} + 3.0 mol L^{-1} H_2SO_4 were used as the negative and positive electrolytes, respectively. In the cycling tests, to maintain a reasonable testing time, 20 mL solutions were used. The electrolytes were circulated at a constant flow rate by a 2-channel peristaltic pump (Longer pump, BT600-2J). The flow rates of the e-fuel charger and the e-fuel cell were 50 and 80 mL min^{-1}, respectively. N_2 gas was bubbled to exhaust the air during all the battery tests. The cell structure and test conditions of VRFBs are the same as those of the e-fuel system.

2.3. Electrochemical measurements

All the electrochemical measurements were conducted on a CHI 660D electrochemical workstation (CH Instruments, Shanghai) in a conventional three-electrode cell, and all the curves were iR corrected. To evaluate the hydrogen evolution reaction of the electrodes, linear sweep voltammetry (LSV) measurements were conducted with the potential scanning from −0.2 to −0.9 V vs. Ag/AgCl at the scan rate of 5 mV s^{-1} in N_2-saturated 0.5 mol L^{-1} H_2SO_4 solution. The prepared graphite felts, graphite rod, and Ag/AgCl (saturated KCl) were adopted as the working, contour, and reference electrodes, respectively. The potentials were converted to that for a reversible hydrogen electrode (RHE) using the formula of E (vs. RHE) = E (vs. Ag/AgCl) + 0.197 + 0.059 pH. Pb was electrodeposited on the HAGF before the LSV tests by adopting the HAGF, platinum mesh, and saturated calomel electrode (SCE) as the working, contour, and reference electrodes, respectively, with a constant current density of 1 mA cm^{-2} for 30 min in 0.1 mol L^{-1} $Pb(SO_3CH_3)_2$ solution. To evaluate the promotion to V^{2+} oxidation reaction, the LSV measurements were conducted with the potential scanning from –0.8 to –0.1 V vs. SCE at the scan rate of 5 mV s^{-1} in a 0.1 mol L^{-1} V^{2+} + 3 mol L^{-1} H_2SO_4 solution. The catalyst-deposited glassy carbon (GC), platinum mesh, and SCE were adopted as the working, contour, and reference electrodes, respectively. The Pb and Bi were electrodeposited on the GC before the LSV tests by adopting GC as the working electrode with a constant current density of 1 mA cm^{-2} for 480 s in 0.1 mol L^{-1} $Pb(SO_3CH_3)_2$ and 0.1 mol L^{-1} $BiCl_3$ + 3 mol L^{-1} HCl solution, respectively. The VRFB and e-fuel system were all tested on an Arbin BT2000 (Arbin Instrument, Inc.) with a charge cutoff voltage of 1.7 V and a discharge cutoff voltage of 1.0 V. To obtain the polarization curves, the e-fuel cell was first charged to 100% SOC, and then polarized at a voltage reduction rate of 50 mV s^{-1}. All the tests were conducted at room temperature (25 °C), unless noted otherwise.

2.4. Computational details

Density functional theory (DFT) based first-principles calculations were performed with the ABINIT [17,18] code. The exchange-correlation function was dealt with by the generalized gradient approximation (GGA) of Perdew-Burke-Ernzerhof (PBE) type [19], and the core electrons were modeled by the projector augmented wave (PAW) method [20]. The energy cutoff was set to 22 Ha for wave-basis expansion, and a vacuum layer of 20 Å was added in the slab models. The slab models for the pristine carbon surface, oxygen functional group, and carbon vacancy were all built on the basis of a monolayer graphite (0 0 0 1) surface in a 4 × 4 × 1 supercell, the feasibility of which had been proven in previous works [21,22]. The slab model of Pb was built based on the close-packed Pb (1 1 1) surface containing three atomic layers with the bottom one fixed. The spacing between k-point grids was all less than 0.05 $Å^{-1}$. The force convergence criteria for self-consistent-field cycles and structural relaxation were 4.0×10^{-5} and 6×10^{-4} Ha $Bohr^{-1}$, respectively.

The hydrogen adsorption energy was calculated by

$$\Delta E_H = E_{(H-electrode)} - E_{(Electrode)} - 1/2E_{(H_2)}, \quad (1)$$

where $E_{(H-electrode)}$ is the total energy for the electrode with a hydrogen atom adsorbed on the surface, $E_{(Electrode)}$ is the total energy for the electrode without hydrogen atom adsorbed on the surface, and $E_{(H_2)}$ is the energy of the gas phase hydrogen molecule. The Gibbs free energy for hydrogen adsorption was obtained from

$$\Delta G_H = \Delta E_H + \Delta E_{ZPE} - T\Delta S_H, \quad (2)$$

where ΔE_{ZPE} and ΔS_H are the zero-point energy difference and entropy between the adsorbed state and the gas phase state, respectively. The overall correction can be approximated to be $\Delta G_H = \Delta E_H + 0.24$ eV [23].

2.5. Calculations of open circuit voltage (OCV)

The OCV is calculated by the Nernst equation incorporating the proton concentration and Donnan potential [24]:

$$E = E_0 + \frac{RT}{F}\ln\left(\frac{c_{VO_2^+} \cdot c_{V^{2+}} \cdot \left(c_{H^+}^+\right)^3}{c_{VO^{2+}} \cdot c_{V^{3+}} \cdot c_{H^+}^-}\right) \quad (3)$$

where E is the OCV, E_0 is the standard potential for VRFBs, R is the universal gas constant, T is the temperature, and F is Faraday's constant. The symbols $c_{V^{2+}}$, $c_{V^{3+}}$, $c_{VO^{2+}}$ and $c_{VO_2^+}$ represent the concentrations of V^{2+}, V^{3+}, VO^{2+}, and VO_2^+, respectively. $c_{H^+}^+$ and $c_{H^+}^-$ are the proton concentrations in the positive and negative electrolytes, respectively. All the initial SOCs were obtained from the experimental OCVs before charge or discharge.

2.6. Cost analysis

The capital cost of the e-fuel system can be divided into the cost of energy, cost of power, and cost of balance of plant. The energy part can be scaled with electrolyte mass, relating to the energy storage capacity of the system. The power part consists of the cost of the e-fuel charger and the cost of the e-fuel cell, determined by the area of the reactors. The capital cost corresponding to the transportation of electrolytes is considered by allocating 1000-m pipes for each user and additional pumps. The surface area of each e-fuel cell (A_{cell}) is calculated by

$$A_{\text{cell}} = \frac{P_{\text{rated-cell}} + P_{\text{loss-cell}}}{i_{\text{discharge}}\bar{U}_{\text{discharge}}}, \quad (4)$$

where $P_{\text{rated-cell}}$ is the rate discharge power, $P_{\text{loss-cell}}$ is the power losses of the e-fuel cell, $i_{\text{discharge}}$ is the discharge current density, and $\bar{U}_{\text{discharge}}$ is the average discharge voltage. The surface area of the e-fuel charger (A_{charger}) is calculated by

$$A_{\text{charger}} = \frac{nt_{\text{discharge}}P_{\text{rated-cell}} + 24P_{\text{loss-charger}}}{24i_{\text{charger}}\bar{U}_{\text{charge}}}, \quad (5)$$

where n is the number of users, $t_{\text{discharge}}$ is the discharge time, $P_{\text{loss-charger}}$ is the power losses of the e-fuel charger, i_{charger} is the charge current density, and $\bar{U}_{\text{charge}}$ is the average charge voltage. The charge time for the e-fuel charger is fixed to be 24 h because the e-fuel charger is able to be continuously operated during the whole day and the e-fuel cell can be operated whenever on demand. The volume of electrolyte (V) is calculated by

$$V = \frac{2nt_{\text{discharge}}P_{\text{rated-cell}}}{\eta\bar{U}_{\text{discharge}}c_aF}, \quad (6)$$

where η is the electrolyte utilization, c_a is the concentration of active species, and F is the Faraday's constant. The power-related cost (C_P) is calculated by

$$C_P = A_{\text{charger}}\sum_i C_{P-\text{charger},i} + C_{P-\text{charger},M} + nA_{\text{cell}}\sum_j C_{P-\text{cell},j} + nC_{P-\text{cell},M} \quad (7)$$

where $C_{\text{P-charger},i}$ is the cost of the power-related components of the e-fuel charger, $C_{\text{P-charger,M}}$ is the manufacturing cost of the e-fuel charger, $C_{\text{P-cell},j}$ is the cost of the power-related components of the e-fuel cell, and $C_{\text{P-cell,M}}$ is the manufacturing cost of the e-fuel cell. The energy-related cost (C_E) is calculated by

$$C_E = \sum_i \frac{c_{a,i}VM_{a,i}Q_{a,i}}{m_{a,i}S_{a,i}} + \sum_j c_{s,j}VM_{s,j}Q_{s,j} + C_{E,M} + 2Q_tV, \quad (8)$$

where $M_{a,i}$ is the molar mass of active materials, $Q_{a,i}$ is the cost of active materials, $m_{a,i}$ is the transferred electrons in the reaction, $S_{a,i}$ is the stoichiometric number of active materials, $M_{s,j}$ is the molar mass of supporting species, $Q_{s,j}$ is the cost of supporting species, $C_{E,M}$ is the manufacturing cost of the energy part, and Q_t is the cost of a tank per volume. The capital cost (C) is, therefore, calculated by

$$C = \frac{C_P + C_E + C_{BOP}}{nt_{\text{discharge}}P_{\text{rated-cell}}}, \quad (9)$$

where C_{BOP} is the cost of balance of plant. The component cost data can be found in the Table S1 (online).

3. Results and discussion

The e-fuel charger, as a power station that continuously converts intermittent electricity into liquid fuels, should be efficient. Therefore, it should be able to minimize the charge overpotential, suppress the side reactions, and reduce the vanadium crossover. Based on these targets, an e-fuel charger has been designed, as shown schematically in Fig. 2a. In the e-fuel charger, the electrode has a high content of oxygen functional groups and high specific surface area (Fig. S1 online) to promote the V^{3+} reduction reaction. And the hydrogen evolution inhibitor is deposited on the negative electrode to suppress the severe hydrogen evolution reaction caused by the highly active electrode. In addition, to enable charging with low current densities and reduce the crossover of vanadium ions, a membrane with low vanadium permeability is adopted. Fig. 2b exhibits the voltage curves for the e-fuel charger at charge current densities ranging from 20 to 120 mA cm^{-2}. Results show that the e-fuel charger has a low charge overpotential and the electroactive species can be nearly fully charged, demonstrating the high utilization of electroactive species in the e-fuel charger.

An energy loss analysis was conducted to evaluate the charge efficiency of the e-fuel charger. The charge efficiency is the ratio between the amount of energy in the charged e-fuels and the electric energy consumed in charging the e-fuels, which can also be defined as the ratio between the theoretical energy needed and the real energy consumed to charge a certain amount of e-fuels. Fig. 2c shows the energy loss analysis results at a charge current density of 60 mA cm^{-2}. Here, the blue line is the OCV at different state of charge (SOC), and the red line is the real charge voltage in charging the e-fuels. Therefore, the area (gray region) between them stands for the energy loss during charge. At the current density of 60 mA cm^{-2}, the theoretical energy needed to charge the e-fuels is calculated to be 19.2 Wh L^{-1}, and the real energy consumed is found to be 20.4 Wh L^{-1}, representing a charge efficiency of as high as 94.4%. The energy loss analysis at the charge current densities of 20, 40, 80, 100 and 120 mA cm^{-2} are shown in Figs. S2–S6 (online), and the corresponding charge efficiencies are summarized in Fig. 2d. It is encouraging to find that the e-fuel charger is able to maintain charge efficiencies of 95.9% to 92.1% at charge current densities from 20 to 120 mA cm^{-2}. These data demonstrate the high conversion rate of electric energy into e-fuels in the e-fuel charger, which are much higher than that of the state-of-art water electrolysis for hydrogen production (60% [25,26]), as shown in Fig. 2e.

The e-fuel cell, as a stand-alone power pack that generates electricity by using charged e-fuels, should be capable of delivering a high power density. Therefore, it should be operated at a high current density, and the voltage losses, including activation, ohmic, and concentration losses, should be minimized. A schematic of the e-fuel cell design is exhibited in Fig. 3a. The e-fuel cell can adopt highly active electrodes with high contents of oxygen functional groups and high specific surface area to promote the vanadium redox reactions, considering that the hydrogen evolution reaction in the discharge is not as severe as that in the charge [27]. Meanwhile, the V^{2+} oxidation promoter is deposited on the negative electrode to further enhance the reaction kinetics of the V^{2+}/V^{3+} redox couple (Fig. S7 online) because it is the limiting step to achieve the high power density [28]. To reduce the ohmic loss and enable the operation at high current densities, a highly proton conductive membrane with high ionic conductivity is used. As a result, the e-fuel cell is able to exhibit a high discharge efficiency and unprecedented peak power density. Fig. 3b shows the discharge voltage curves in the e-fuel cell at various current densities, and the corresponding charge current densities in the e-fuel charger are graphed in Fig. S8 (online). Here, the charge current density in the e-fuel charger is fixed at 60 mA cm^{-2} and the discharge current density in the e-fuel cell ranges from 400 to 1,200 mA cm^{-2}. It is seen that the e-fuel cell maintains high onset voltages, which range from 1.47 V at 400 mA cm^{-2} to 1.25 V at 1,200 mA cm^{-2}, and high specific capacities, which range from 13.7 Ah L^{-1} at 400 mA cm^{-2} to 11.2 Ah L^{-1} at 1,200 mA cm^{-2}.

An energy loss analysis was also conducted to evaluate the discharge efficiency of the e-fuel cell, which is defined as the ratio between the real energy output and the theoretical energy in the charged e-fuels. The results are shown in Figs. S9–S13 (online). Similar to the energy loss in the charge process, the area between the OCV and real discharge voltage stands for the energy loss during discharge. As shown in Fig. 3c, discharge efficiency ranges from 97.0% at 400 mA cm^{-2} to 83.1% at 1,200 mA cm^{-2}. Fig. 3d exhibits the polarization curves and the corresponding power densities of the e-fuel cell. As shown in Fig. 3e, the e-fuel cell is capable of

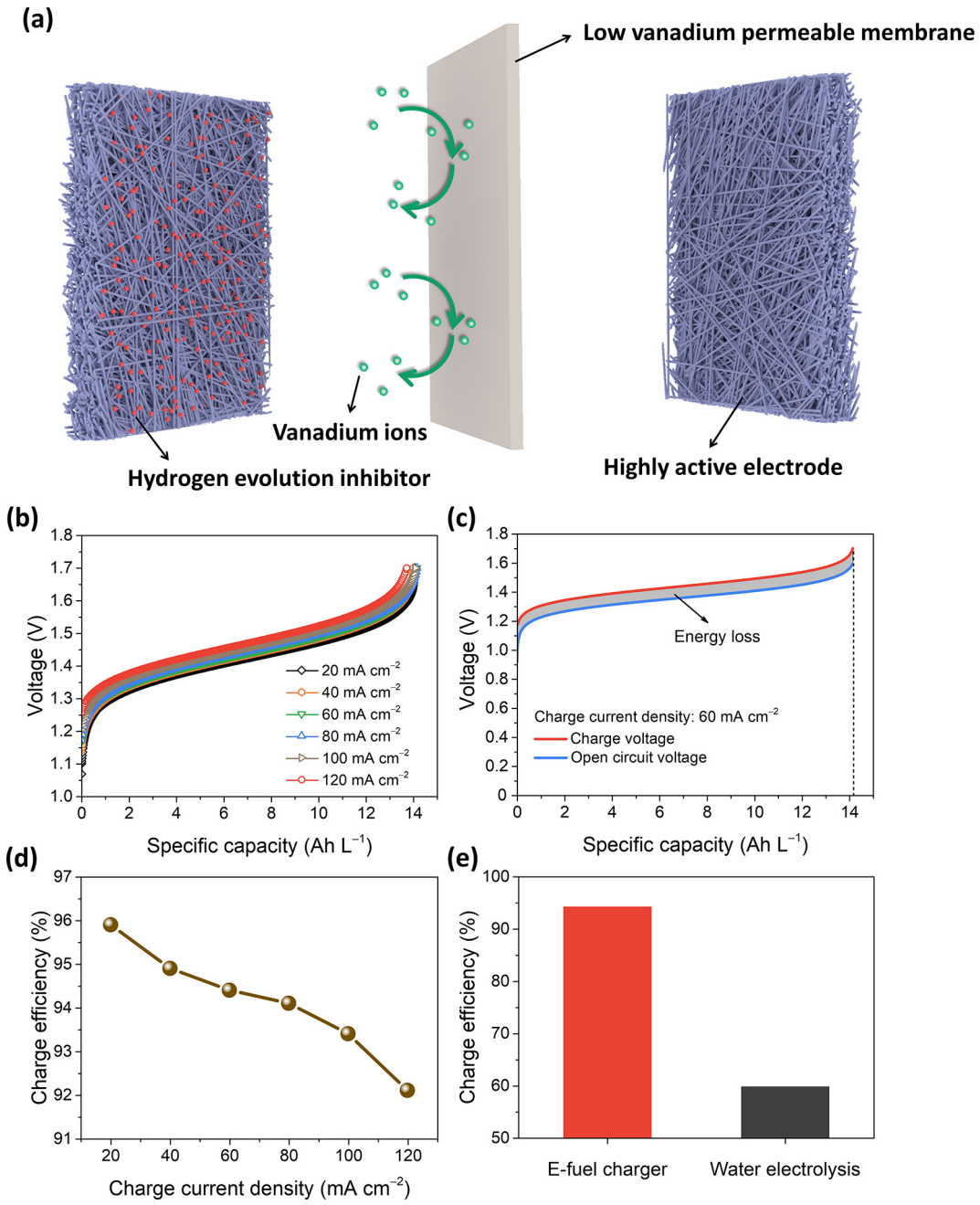

Fig. 2. Design and performance of the e-fuel charger. (a) Schematic of the e-fuel charger design. (b) Charge voltage curves of the e-fuel charger at varying charge current densities. (c) Energy loss analysis of the e-fuel charger at the charge current density of 60 mA cm^{-2}. (d) Charge efficiencies at varying charge current densities. (e) Comparison of efficiency of the e-fuel charger and water electrolysis.

delivering a high peak power density of 3.4 W cm^{-2} with a limiting current density of ~9,000 mA cm^{-2}, which is several times higher than that of the proton exchange membrane (PEM) fuel cell (1.27 W cm^{-2} [29]), direct ethanol fuel cell (0.24 W cm^{-2} [30]), direct methanol fuel cell (0.13 W cm^{-2} [31]), and zinc-air fuel cell (0.27 W cm^{-2} [32]). These results demonstrate that the e-fuel cell holds the potential for not only grid-scale energy storage, but also next-generation vehicles, especially when adopting e-fuels with high energy density.

To offer a more comprehensive understanding of the whole e-fuel system, we calculated the round-trip efficiency and electrolyte utilization and compared the results with those of a VRFB at the same operating condition. Schematics of the VRFB and e-fuel system are shown in Fig. 4a and b, respectively, while digital photos of a VRFB and e-fuel system are shown in Figs. S14 and S15 (online). As shown in Fig. 4a for the VRFB, for the V^{2+}/V^{3+} redox couple, the oxidation of V^{2+} and the reduction of V^{3+} take place on the same electrode surface, but for the e-fuel system shown in Fig. 4b, the oxidation and reduction reactions occur separately on different electrode surfaces, with one in the e-fuel charger and the other in the e-fuel cell. Comparisons of round-trip efficiency and electrolyte utilization for the VRFB and e-fuel system are presented in Figs. 4c and d. Again, the charge current density for both systems is 60 mA cm^{-2}, and the discharge current densities range from 400 to 1,200 mA cm^{-2}. The charge-discharge voltage curves of the VRFB are shown in Fig. S16 (online) and those of e-fuel system are exhibited in Figs. 3b and S8 (online). These results show that the e-fuel system outdistances the VRFB, and

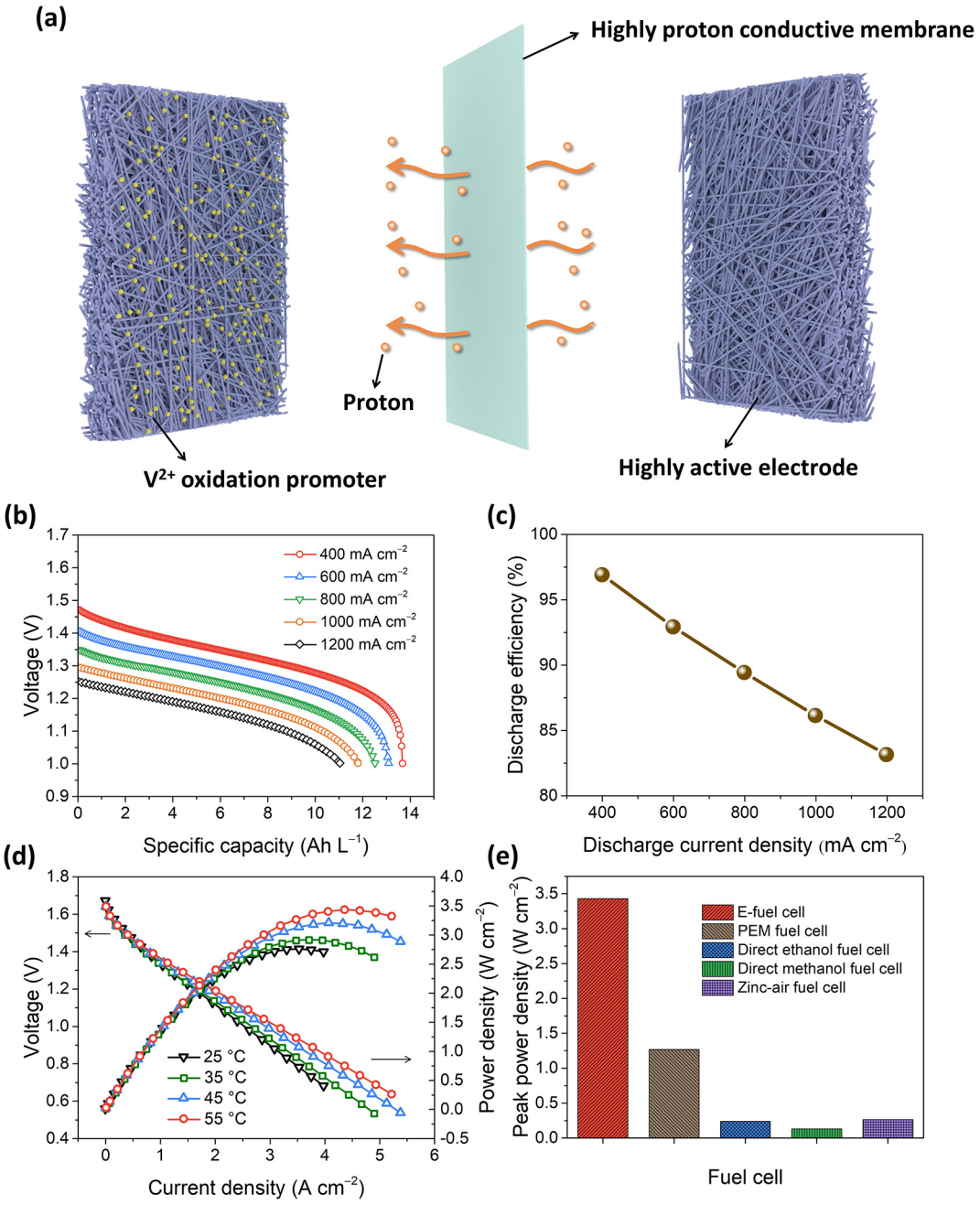

Fig. 3. Design and performance of the e-fuel cell. (a) Schematic of the e-fuel cell design. (b) Discharge voltage curves at varying discharge current densities. (c) Discharge efficiencies at varying discharge current densities. (d) Polarization curves and power densities of the e-fuel cell at varying temperatures. (e) Comparison of peak power density for the e-fuel cell and other representative fuel cells.

achieves unprecedented round-trip efficiencies and electrolyte utilizations. At the discharge current densities of 400, 600 and 800 mA cm^{-2}, the round-trip efficiencies for the e-fuel system are 88.4%, 85.5%, and 82.7%, which are 11.2%, 13.5%, and 16.3% higher than those of the VRFB, respectively. Even at the ultra-high discharge current densities of 1,000 and 1,200 mA cm^{-2}, the e-fuel system can still exhibit round-trip efficiencies of 80.0% and 77.2%, representing the most efficient energy storage system in the open literature. More remarkably, the e-fuel system can maintain high electrolyte utilizations during operation, which can greatly reduce the use of precious active materials and decrease the capital cost of the system. At the discharge current densities of 400, 600, 800 and 1,000 mA cm^{-2}, the e-fuel system exhibits high electrolyte utilizations of 95.7%, 91.8%, 87.9%, and 83.0%, which are 32.7%, 41.8%, 54.4% and 67.3% higher than those of the VRFB, at current densities of 400, 600, 800 and 1,000 mA cm^{-2}, respectively. These results further demonstrate the superiority of the e-fuel system to the state-of-art electrical energy storage systems.

In addition to the consideration of performance, the widespread application of the e-fuel system will also be decided by economic factors. Thus, a cost analysis was conducted for a micro-grid community in which each user has a 5 kW power supply for several hours per day. The objective was to evaluate and compare the capital cost of the e-fuel system and VRFB. The cost model and component prices adopted here are based on previous research [33–35], and adjustments are made for the e-fuel system to incorporate the decoupled charge and discharge processes. The performance of VRFB was obtained from the typical galvanostatic charge-

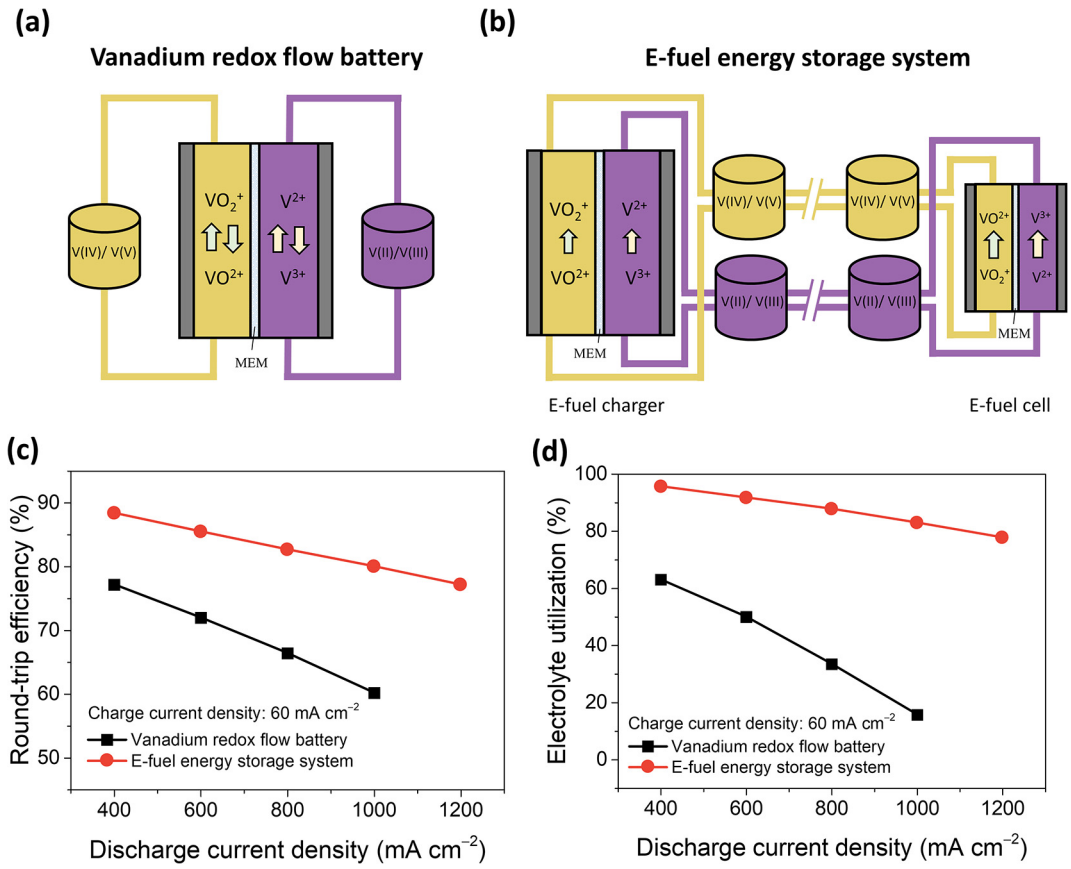

Fig. 4. Schematics of setup of the (a) vanadium redox flow battery and (b) e-fuel energy storage system. Comparison of the (c) round-trip efficiency and (d) electrolyte utilization for the vanadium redox flow battery and e-fuel energy storage system.

discharge tests, and the charge-discharge voltage curves as well as the corresponding efficiencies are shown in Fig. S17 (online). For the e-fuel system, because the charge and discharge processes are decoupled and can be operated simultaneously, the e-fuel charger is able to be operated uninterruptedly for the whole day, while the e-fuel cell can generate electricity whenever needed. Fig. 5a shows the capital costs as a function of the number of users for the VRFB and e-fuel system at 5 kW/10 kWh per user. Results show that although the e-fuel system requires more modules than a VRFB system, its capital cost is lower than the VRFB due to the higher power density, higher electrolyte utilization and higher design flexibility. The data indicate that the capital cost of the VRFB does not change as the number of users increases. This is attributed to the charge and discharge processes taking place in the same stack located at the user side. For the e-fuel system, the capital cost decreases as the number of users increases (from 332.7 $ kWh^{-1} for 1 user to 311.9 $ kWh^{-1} for 20 users), because the capital cost added by an additional e-fuel charger is gradually offset by the increased number of high-performance e-fuel cells. If the number of users is 10, the capital cost of the e-fuel system is calculated to be 313.0 $ kWh^{-1}, which is 27.0% lower than that of the VRFB (428.9 $ kWh^{-1}). The cost breakdown of both systems for 10 users is shown in Fig. 5b. The data show that in the e-fuel system, the cost of stacks is only responsible for a very low fraction of the capital cost, ascribed to the fact that the e-fuel cell is able to be operated at high power densities with small stack size. Figs. 5c and d present the capital costs as a function of the number of users, at 5 kW/20 kWh per user, and the corresponding cost breakdown for 10 users. Results show that as the energy-to-power ratio increases, the capital cost decreases for both the VRFB and e-fuel system. For 20 users, the capital cost of the e-fuel system is 253.7 $ kWh^{-1}, which is 14.3% lower than the 295.9 $ kWh^{-1} for the VRFB. The results at higher energy-to-power ratios of 6 and 8 are shown in Fig. S18 (online), which further demonstrates that the e-fuel system is more cost-effective than the VRFB. In addition, results also show that the cost of electroactive species accounts for a large fraction of the capital cost of the e-fuel system, because the costly vanadium redox couples are used as an example e-fuel here. Considering that cheaper rechargeable species can be used as e-fuels, and the operation time of the e-fuel charger can be much longer than the e-fuel cell in actual operation, the future e-fuel system still has room for further cost reduction.

The source of the e-fuel system outdistancing the VRFB in round-trip efficiency, electrolyte utilization, and capital cost can be ascribed to the independent design, optimization, and operation of the e-fuel charger and e-fuel cell. In the VRFB, although the electrodes with high content of oxygen functional groups and high specific surface area can benefit the vanadium redox reactions, these factors inevitably accelerate the undesirable hydrogen evolution reactions, especially in charge [27,36]. To avoid the fast capacity decay and enable long-term stable operation, the traditional electrodes of the VRFB are generally activated by moderate thermal treatment [37] or acid treatment [38], which can enhance the hydrophily, content of oxygen functional groups along with the specific surface area, while avoiding the severe hydrogen evolution. However, this method also hinders the further reduction in charge overpotential, limiting the enhancement in round-trip efficiency and electrolyte utilization.

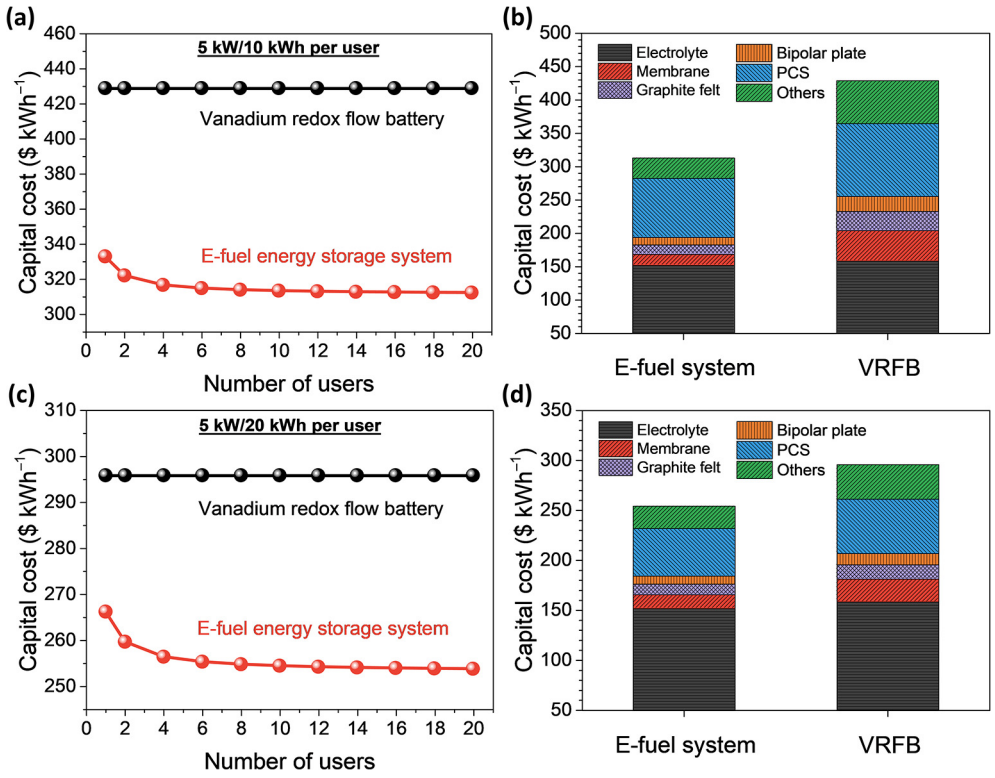

Fig. 5. Cost analysis of the e-fuel system and VRFB. (a) Capital costs as a function of the number of users for the VRFB and e-fuel system at 5 kW/10 kWh per user. (b) Cost breakdown of the VRFB and e-fuel system at 5 kW/10 kWh per user for 10 users. (c) Capital costs as a function of number of users for the VRFB and e-fuel system at 5 kW/20 kWh per user. (d) Cost breakdown of the VRFB and e-fuel system at 5 kW/20 kWh per user for 10 users.

Use of a hydrogen evolution inhibitor on the carbon surface can decouple the link between carbon surface properties and hydrogen evolution reaction, and thus enable the use of highly active electrodes with high content of oxygen functional group and high specific surface area to promote vanadium redox reactions. Figs. 6(a1–a4) show the most stable structures for hydrogen atom adsorbed on a pristine carbon surface, oxygen functional group, carbon vacancy, and Pb (1 1 1) surface, and Fig. 6b exhibits the calculated Gibbs free energies in a three-state diagram. The atomic structures of substrates can be found in Figs. S19 and S20 (online). For substrates with high hydrogen evolution activity, the Gibbs free energy for dissociative adsorption of H_2 (ΔG_H) is close to zero [39]. The ΔG_H of the pristine carbon surface is as large as 1.59 eV, indicating that the pristine carbon surface is inert to the hydrogen evolution reaction. However, when an oxygen functional group and carbon vacancy exist, the ΔG_H decreases to −0.17 and −0.04 eV, respectively, which would greatly enhance the hydrogen evolution reaction, consistent with previous experimental results [27,40]. Interestingly, on the Pb surface, the ΔG_H increases to 0.92 eV, suggesting that Pb can be an efficient hydrogen evolution inhibitor that limits the hydrogen evolution reaction. Based on this finding, linear sweep voltammetry tests were conducted to demonstrate the effect of Pb on the highly active electrode. Figs. 6c and 6d present the iR-corrected LSV curves and Tafel plots for a traditional VRFB electrode, highly active electrode, and Pb-modified highly active electrode. The traditional VRFB electrode (Fig. S21 online) shows a low current density and a high Tafel slope of 573 mV dec^{-1}, indicating that it is inert to the hydrogen evolution reaction during operation. However, for a highly active electrode, due to the existence of abundant oxygen functional groups and carbon vacancies (Fig. S1 online), the hydrogen evolution is greatly promoted, as evidenced by a much higher current density and lower Tafel slope of 340 mV dec^{-1}. After depositing Pb on the highly active electrode, the current density in the LSV curve is obviously reduced and the Tafel slope is increased to 443 mV dec^{-1}, further demonstrating that Pb can effectively suppress the hydrogen evolution reaction for a highly active electrode. Although a hydrogen evolution inhibitor enables the use of a highly active electrode in the charge, its application in the VRFB is hindered as Pb undergoes irreversible dissolution before V^{2+} oxidation in the discharge, as shown in Fig. S22 (online). On the contrary, the dissolution of the hydrogen evolution inhibitor is not an issue in the e-fuel system, because the discharge does not happen at the same electrode as the charge. This enables the adoption of a highly active electrode to lower the overpotential and avoid severe side reactions.

In addition to the separated electrode design, another method to lower the charge overpotential and allow more electroactive species to be charged below the cutoff voltage is to reduce the charge current density. However, in the VRFB, charging the electroactive active species at a low current density would increase the crossover, lower the coulombic efficiency, and accelerate the capacity decay rate, due to the prolonged charge time. Figs. 7a and b show the cycling performance at charge and discharge current densities of 60 and 600 mA cm^{-2} for a VRFB with a highly proton conductive membrane (*e.g.*, thin membrane), which can ensure a high power density in the discharge. However, the results show that the battery exhibits a low coulombic efficiency of ~95% and fast capacity decay rate of 0.9% per cycle, indicating this kind of design and operating condition is not suitable for long-term VRFB operation. One method to alleviate the crossover issue in the charge is to use a membrane with low vanadium permeability (*e.g.*, thick membrane), but that would reduce the proton conductivity across the membrane and increase the ohmic loss of the bat-

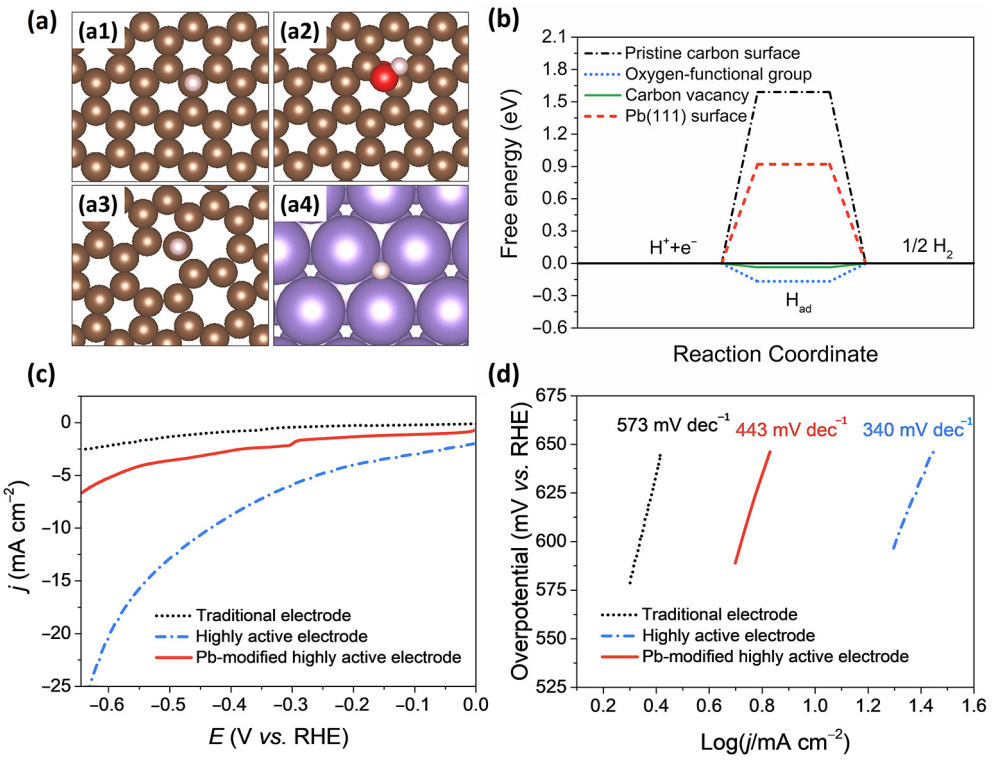

Fig. 6. Comparison of the electrode for the e-fuel system and VRFB. (a1–a4) Most stable structures of hydrogen atom adsorbed on pristine carbon surface, oxygen functional group, carbon vacancy and Pb (1 1 1) surface. The brown, white, red and purple balls represent carbon, hydrogen, oxygen and lead atoms, respectively. (b) Calculated Gibbs free energies in a three-state diagram for pristine carbon surface, oxygen functional group, carbon vacancy, and Pb (1 1 1) surface. (c and d) The iR-corrected LSV curves and Tafel plots for traditional electrode, highly active electrode, and Pb-modified highly active electrode in an N_2-saturated 0.5 mol L^{-1} H_2SO_4 solution at the scan rate of 5 mV s^{-1}.

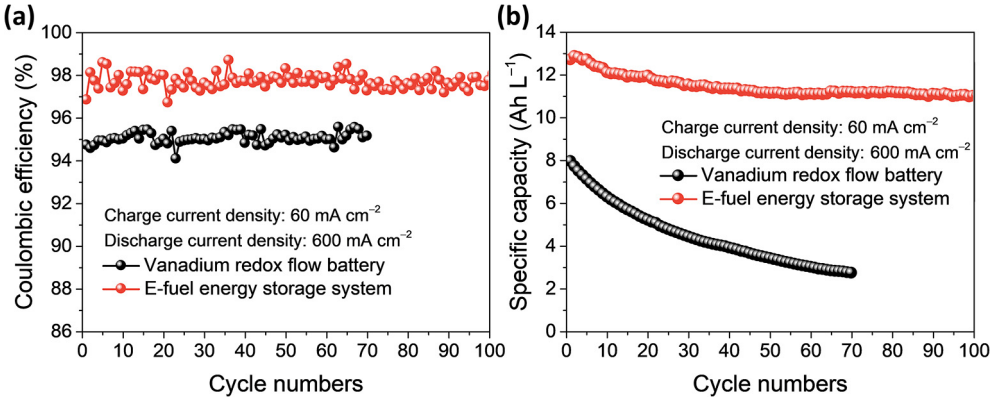

Fig. 7. Comparison of the membrane for the e-fuel system and VRFB. (a) Coulombic efficiency and (b) discharge specific capacity for the VRFB and e-fuel system during cycling at charge and discharge current densities of 60 and 600 mA cm^{-2}.

tery, leading to a low power density in the discharge process. The e-fuel system avoids these problems. The e-fuel charger is operated at low current density with a low vanadium permeability membrane, which can reduce the charge overpotential and avoid the enhanced crossover of active species, while the e-fuel cell is discharged at high current density with a high proton conductive membrane, ensuring the high power density of the power stack. With this novel design, the e-fuel system can be operated for more than 100 cycles with a high coulombic efficiency of ~98% and a capacity decay rate of only 0.1% per cycle, as shown in Figs. 7a and b, demonstrating the system's high stability for long-term operation.

4. Conclusion

We propose a novel e-fuel energy storage system that incorporates electrically rechargeable liquid fuels as the storage medium. This e-fuel system is efficient, scalable, durable, cost-effective, and site-independent, and it can be continuously operated. We then demonstrate an example e-fuel system with V^{2+}/V^{3+} and VO^{2+}/VO_2^+ redox couples. The e-fuel charger achieved a charge efficiency of ~94%, which is 56% higher than that for hydrogen production by water electrolysis, and the e-fuel cell delivered a peak power density of 3.4 W cm^{-2}, which is 2.7 times of that of hydrogen fuel cells. In addition, the e-fuel system achieved a round-

trip efficiency of 80.0% and an electrolyte utilization of 83.0% at an ultra-high discharge current density of 1,000 mA cm^{-2}, making it to be the most efficient energy storage system in the open literature. This unprecedented performance allows a 27.0% reduction in the capital cost of the e-fuel system compared to the traditional VRFBs in large-scale energy storage. It is also important to note that the e-fuels composed of V^{2+}/V^{3+} and VO^{2+}/VO_2^+ redox couples are examples demonstrated in the present work. The proposed concept of the e-fuel energy storage, which enables decoupling of charge and discharge, will allow exploration of a number of e-fuels, which are energy dense, efficient, stable, flowable, and cost effective. The electroactive materials for e-fuels can range from inorganic, organic, and suspensions of solid particles (nanofluid e-fuels). The super performance demonstrated in the present work suggests that the e-fuel energy storage system has the potential to revolutionize energy storage technology and substantially facilitates the adoption and deployment of renewable energy.

Conflict of interest

The authors declare that they have no conflict of interest.

Acknowledgments

This work was fully supported by the Grant from the Research Grant Council of the Hong Kong Special Administrative Region, China (T23-601/17-R).

Author contributions

T.Z. conceived the idea of the e-fuel storage and supervised the project. H.J., L.W. and T.Z. designed the experiments. H.J. performed the experiments and analyzed the data. L.W. helped with the cost analysis. X.F. and J.X. helped with electrochemical measurements. W.S. provided scientific advice during the project. T.Z. H.J., L.W., X.F., J.X., W.S. and T.Z. contributed to writing the manuscript. All of the authors discussed the results and commented on the manuscript.

Appendix A. Supplementary data

Supplementary data to this article can be found online at https://doi.org/10.1016/j.scib.2019.01.014.

References

[1] Bodansky D. The Paris climate change agreement: a new hope? Am J Int Law 2016;110:288–319.
[2] Branker K, Pathak M, Pearce JM. A review of solar photovoltaic levelized cost of electricity. Renewable Sustainable Energy Rev 2011;15:4470–82.
[3] Deane JP, Gallachóir BÓ, McKeogh E. Techno-economic review of existing and new pumped hydro energy storage plant. Renewable Sustainable Energy Rev 2010;14:1293–302.
[4] Swider DJ. Compressed air energy storage in an electricity system with significant wind power generation. IEEE Trans Energy Convers 2007;22:95–102.
[5] Zhang LL, Zhao X. Carbon-based materials as supercapacitor electrodes. Chem Soc Rev 2009;38:2520–31.
[6] Tarascon J, Armand M. Issues and challenges facing rechargeable lithium batteries. Nature 2001;414:359–67.
[7] Soloveichik GL. Flow batteries: current status and trends. Chem Rev 2015;115:11533–58.
[8] Jiang H, Shyy W, Wu M, et al. A bi-porous graphite felt electrode with enhanced surface area and catalytic activity for vanadium redox flow batteries. Appl Energy 2019;233:105–13.
[9] Chen H, Cong TN, Yang W, et al. Progress in electrical energy storage system: a critical review. Prog Nat Sci 2009;19:291–312.
[10] Satyapal S, Petrovic J, Read C, et al. The US department of energy's national hydrogen storage project: progress towards meeting hydrogen-powered vehicle requirements. Catal Today 2007;120:246–56.
[11] Felderhoff M, Weidenthaler C, von Helmolt R, et al. Hydrogen storage: the remaining scientific and technological challenges. Phys Chem Chem Phys 2007;9:2643–53.
[12] Durbin D, Malardier-Jugroot C. Review of hydrogen storage techniques for on board vehicle applications. Int J Hydrogen Energy 2013;38:14595–617.
[13] Li Y, Feng Y, Sun X. Insight into interface behaviors to build phase-boundary-matched Na-Ion direct liquid fuel cells. ACS Sustainable Chem Eng 2018;6:12827–34.
[14] Luo Q, Li L, Wang W, et al. Capacity decay and remediation of Naion-based all-vanadium redox flow batteries. ChemSusChem 2013;6:268–74.
[15] Jiang H, Shyy W, Zeng L, et al. Highly efficient and ultra-stable boron-doped graphite felt electrodes for vanadium redox flow batteries. J Mater Chem A 2018;6:13244–53.
[16] Jiang H, Shyy W, Wu M, et al. Highly active, bi-functional and metal-free B_4C-nanoparticle-modified graphite felt electrodes for vanadium redox flow batteries. J Power Sources 2017;365:34–42.
[17] Gonze X, Beuken J, Caracas R, et al. First-principles computation of material properties: the ABINIT software project. Comput Mater Sci 2002;25:478–92.
[18] Gonze X. A brief introduction to the ABINIT software package. Z Kristallogr 2005;220:558–62.
[19] Perdew JP, Burke K, Ernzerhof M. Generalized gradient approximation made simple. Phys Rev Lett 1996;77:3865.
[20] Kresse G, Joubert D. From ultrasoft pseudopotentials to the projector augmented-wave method. Phys Rev B 1999;59:1758.
[21] Jiang H, Wu M, Ren Y, et al. Towards a uniform distribution of zinc in the negative electrode for zinc bromine flow batteries. Appl Energy 2018;213:366–74.
[22] Jiang H, Tan P, Liu M, et al. Unraveling the positive roles of point defects on carbon surfaces in nonaqueous lithium-oxygen batteries. J Phys Chem C 2016;120:18394–402.
[23] Zhang L, Liu W, Dou Y, et al. The role of transition metal and nitrogen in metal-N-C composites for hydrogen evolution reaction at universal pHs. J Phys Chem C 2016;120:29047–53.
[24] Knehr K, Kumbur E. Open circuit voltage of vanadium redox flow batteries: discrepancy between models and experiments. Electrochem Commun 2011;13:342–5.
[25] Feng Q, Liu G, Wei B, et al. A review of proton exchange membrane water electrolysis on degradation mechanisms and mitigation strategies. J Power Sources 2017;366:33–55.
[26] Buttler A, Spliethoff H. Current status of water electrolysis for energy storage, grid balancing and sector coupling via power-to-gas and power-to-liquids: a review. Renewable Sustainable Energy Rev 2018;82:2440–54.
[27] Schweiss R, Pritzl A, Meiser C. Parasitic hydrogen evolution at different carbon fiber electrodes in vanadium redox flow batteries. J Electrochem Soc 2016;163:A2089–94.
[28] Agar E, Dennison C, Knehr K, et al. Identification of performance limiting electrode using asymmetric cell configuration in vanadium redox flow batteries. J Power Sources 2013;225:89–94.
[29] Klingele M, Breitwieser M, Zengerle R, et al. Direct deposition of proton exchange membranes enabling high performance hydrogen fuel cells. J Mater Chem A 2015;3:11239–45.
[30] An L, Zhao T, Chen R, et al. A novel direct ethanol fuel cell with high power density. J Power Sources 2011;196:6219–22.
[31] Katzfuß A, Gogel V, Jörissen L, et al. The application of covalently cross-linked BrPPO as AEM in alkaline DMFC. J Membr Sci 2013;425:131–40.
[32] Li Y, Gong M, Liang Y, et al. Advanced zinc-air batteries based on high-performance hybrid electrocatalysts. Nat Commun 2013;4:1805.
[33] Viswanathan V, Crawford A, Stephenson D, et al. Cost and performance model for redox flow batteries. J Power Sources 2014;247:1040–51.
[34] Crawford A, Viswanathan V, Stephenson D, et al. Comparative analysis for various redox flow batteries chemistries using a cost performance model. J Power Sources 2015;293:388–99.
[35] Zeng Y, Zhao T, An L, et al. A comparative study of all-vanadium and iron-chromium redox flow batteries for large-scale energy storage. J Power Sources 2015;300:438–43.
[36] Shah A, Al-Fetlawi H, Walsh F. Dynamic modelling of hydrogen evolution effects in the all-vanadium redox flow battery. Electrochim Acta 2010;55:1125–39.
[37] Kim KJ, Kim Y, Kim J, et al. The effects of surface modification on carbon felt electrodes for use in vanadium redox flow batteries. Mater Chem Phys 2011;131:547–53.
[38] Yue L, Li W, Sun F, et al. Highly hydroxylated carbon fibres as electrode materials of all-vanadium redox flow battery. Carbon 2010;48:3079–90.
[39] Zhang L, Chen Y, Zhao P, et al. Fe_3C Nanorods encapsulated in N-doped carbon nanotubes as active electrocatalysts for hydrogen evolution reaction. Electrocatalysis 2018;9:264–70.
[40] Li W, Liu J, Yan C. Reduced graphene oxide with tunable C/O ratio and its activity towards vanadium redox pairs for an all vanadium redox flow battery. Carbon 2013;55:313–20.

Haoran Jiang obtained his B.E. degree (2014) from Huazhong University of Science and Technology, and Ph.D. degree (2018) from Hong Kong University of Science and Technology. He is currently a Postdoctoral Fellow at the Department of Mechanical and Aerospace Engineering of HKUST. His research mainly focuses on the coupled transport and electrochemical phenomena in redox flow batteries, and advanced modeling.

Tianshou Zhao is a Cheong Ying Chan Professor of Engineering and Environment, Chair Professor of Mechanical and Aerospace Engineering, Director of the HKUST Energy Institute, Senior Fellow of the HKUST Institute for Advanced Study, elected Fellow of the American Society Mechanical Engineers (ASME), Fellow of the Royal Society of Chemistry (RSC), and Highly Cited Researcher in Engineering by Thomson Reuters (2014–2018). His research mainly focuses on fuel cells, advanced batteries, multi-scale multiphase heat and mass transport with electrochemical reactions, and computational modeling.